Stoch Environ Res Risk Assess (2011) 25:697–711
DOI 10.1007/s00477-011-0479-3

ORIGINAL PAPER

Ecological risk assessment for water scarcity in China's Yellow River Delta Wetland

Yan Qin · Zhifeng Yang · Wei Yang

Published online: 27 April 2011

Abstract Wetlands are ecologically important due to their hydrologic attributes and their role as ecotones between terrestrial and aquatic ecosystems. Based on a 2-year study in the Yellow River Delta Wetland and a Markov-chain Monte Carlo (MCMC) simulation, we discovered temporal and spatial relationships between soil water content and three representative plant species (*Phragmites australis* (Cav.) Trin. ex Steud., *Suaeda salsa* (Linn.) Pall, and *Tamarix chinensis* Lour.). We selected eight indices (biodiversity, biomass, and the uptake of TN, TP, K, Ca, Mg, and Na) at three scales (community, single plant, and micro-scale) to assess ecological risk. We used the ecological value at risk (EVR) model, based on the three scales and eight indices, to calculate EVR and generate a three-level classification of ecological risk using MCMC simulation. The high-risk areas at a community scale were near the Bohai Sea. The high-risk areas at a single-plant scale were near the Bohai Sea and along the northern bank of the Yellow River. At a micro-scale, we found no concentration of high-risk areas. The results will provide a foundation on which the watershed's planners can allocate environmental flows and guide wetland restoration.

Keywords Ecological risk assessment · EVR model · Water scarcity · Yellow River Delta Wetland

Y. Qin · Z. Yang (✉) · W. Yang
State Key Laboratory of Water Environment Simulation, School of Environment, Beijing Normal University, 19 Xinjiekouwai Street, Beijing 100875, China
e-mail: zfyang@bnu.edu.cn

1 Introduction

Wetlands are ecologically important due to their hydrologic attributes and their role as an ecotone between terrestrial and aquatic ecosystems (Pascoe 1993). Scientists around the world have noted alarming changes in these important ecosystems. Ecological risk assessment provides a scientific foundation for managing the risks that will result from such changes in projects designed to protect and conserve natural ecosystems and biodiversity; the importance of such tools has increasingly been recognized by both academic researchers and environmental managers. There are three main sources of risk that are commonly considered in wetlands research: heavy metals and non-metal elements, such as Cd, Cr, Cu, Hg, Ni, Pb, Zn, As, Bo, and Se (Powell et al. 1997; Overesch et al. 2007; Pollard et al. 2007; Suntornvongsaul et al. 2007; Nabulo et al. 2008; Bai et al. 2010; Brix et al. 2010); organic pollutants, such as heavy oil compounds and persistent organic pesticides (Ji et al. 2007; Chen et al. 2008; Dimitriou et al. 2008; Rumbold et al. 2008; Gao et al. 2009; Yang et al. 2009b); and natural parameters such as water availability and salinity (Speelmans et al. 2007; Sun et al. 2009; Xie et al. 2011). Since water is the defining feature of wetlands, and is essential to their health, water risks take the form of too much or too little water—flooding and drought (Ni and Xue 2003; Smith et al. 2003; Bouma et al. 2005; Cai et al. 2009; Huber et al. 2009; Nicolosi et al. 2009). Most researchers have focused on water scarcity in wetlands at a macro scale (Bouma et al. 2005; Sun et al. 2008; Huber et al. 2009; Yang et al. 2009a), but there has been little research on the risk to wetland species caused by drought (Smith et al. 2003) because wetlands (by definition) mostly have sufficient water. However, drought is an important problem in wetlands in areas where regional drought or

excessive withdrawals of water upstream of a wetland reduce the environmental flows below the level required to sustain wetland health. In this paper, we focused on assessment of the ecological risks that result from water scarcity; that is, we assessed the ecological risk caused by water scarcity. However, because some wetland plants cannot survive long-term flooding, we also considered the risk caused by excess water.

The value at risk (VaR) model was first used in economics research to assess the insurance, investment, and stock risks arising from ecosystem changes by Morgan Guaranry Trust Company (1996). In recent years, it has been used in ecological research from a primarily ecological rather than economic perspective (Shi et al. 2004); for example, ecological value at risk (EVR) has been used to assess the risk to fisheries resources caused by reduced water volumes (Webby et al. 2007). This research demonstrated that the models and concepts of VaR are adaptable to ecological systems in the form of EVR. Many methods have been used to calculate EVR, with different methods suitable for different conditions, datasets, and precision requirements. In general, these can be classified into three types (Dowd 1998): variance–covariance methods, historical simulation methods, and Monte Carlo simulation methods. The Monte Carlo simulation methods appear to be most suitable for ecosystem research because they are inherently probabilistic, and therefore account for the stochastic nature of ecosystems (Srinivasan and Shah 2000; Alexander 2002).

In this paper, we analyzed data for plants and soils in China's Yellow River Delta Wetland using the Markov-chain Monte Carlo (MCMC) method. We classified soil water content in the wetland into three availability levels (drought, sufficient, and flooding) and examined the impacts of these levels on several ecosystem indices, at three different scales (community, single plant, and micro-scale). Based on these results, we calculated the ecological risk to the wetland posed by each of the three water availability levels using the EVR model.

2 Materials and methods

2.1 Study area

The Yellow River Delta (118°33′E to 119°20′E, and 37°35′N to 38°12′N), the world's fastest-growing delta, is located in northeastern Shandong Province, on the southern shore of the Bohai Sea (Fig. 1). The region has a temperate, semi-humid, continental monsoon climate. The average annual temperature is 12.1°C. The average annual precipitation is 552 mm, of which 70% falls during the summer. However, the average annual evaporation is 1962 mm. Since the early 1970s, flow in the Yellow River has been decreasing due to a combination of drought and excessive withdrawals in upstream regions, and the frequency of complete drying or ephemeral flow has been increasing (Liu and Zhang 2002). The worst flow interruption occurred in 1997, when there was no flow in the Yellow River for 226 days (Yang and Yang 2010). During the past 30 years, the wetlands in the Yellow River Delta decreased in extent by more than 300 km^2 (Zong et al.

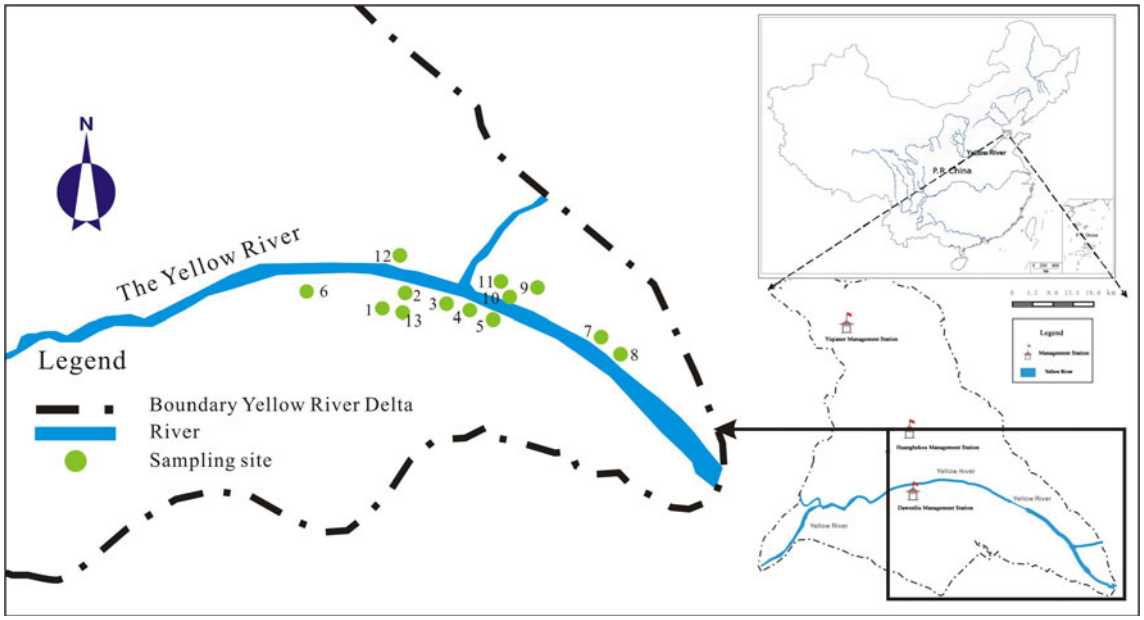

Fig. 1 Locations of the study area and the sampling sites

2008). Water scarcity is therefore one of the biggest threats to the wetland's biodiversity and to plant growth in the wetland.

2.2 Study design

To study the ecological risk of the wetland at three scales, we choose reeds (*Phragmites australis* (Cav.) Trin. ex Steud.), suaeda (*Suaeda salsa* (Linn.) Pall), and saltcedar (*Tamarix chinensis* Lour.) as our study species. These three plants are the most widely distributed and representative species in the delta (He et al. 2009).

2.2.1 Soils and plants

The field study was carried out in the spring, summer, and autumn (from April to October) in 2008 and 2009, because all the plants in the wetlands are dead or dormant during the winter and do not resume growth until April. We selected 13 sampling sites for investigation, each 30 × 30 m, which previous studies have shown to be a suitable scale for the study area (Xiao et al. 2001). At each site, we randomly established 10 quadrats (each 1 × 1 m). Figure 1 shows the locations of the sampling sites.

At each site, we counted the number of species and used this data to represent the biodiversity. We also collected plant and soil samples from all 130 quadrats. In each quadrat, we collected all the aboveground plant parts to measure the total biomass. We separated the reeds, suaeda, and saltcedar so that we could determine separate biomass values for each species. We also obtained two soil samples from each site at a depth of 30 cm: one was stored in a sealed aluminum sample box and used to calculate soil water content, and the other was stored in a plastic bag and used to determine various element contents. In addition, we obtained soil samples at 20-cm depth intervals until we reached the water table at each site. We also installed a neutron probe access tube at site 13, which was the most representative of the sites, so that we could measure soil water content at 10-cm intervals to a depth of 150 cm every 10 days.

2.2.2 Data analysis

Plant and soil samples were air-dried for 20 days, then the dry soil samples were ground with a mortar and pestle and passed through a 100 mesh-sieve (particle size <154 μm) to provide samples with a homogeneous particle size and size distribution. Dry plant samples were mechanically ground (FW100, Anrui, Shanghai, China) to pass through a 1-mm sieve, and were then stored in dark vials until analysis. The plant samples were digested in ultrapure HNO_3 (p.a. 65%) and HF (p.a. 45%), in a 2:1 v/v ratio, whereas soil samples were digested in ultrapure HNO_3 (p.a. 65%) and HClO (p.a. 70%) in a 2:1 v/v ratio. Element concentrations (P, K, Ca, Mg, Na) in soils and plants were measured by means of inductively coupled plasma-emission mass spectrometry (JY-ULTIMA spectrometer, Jobin–Yvon, Longjumeau, France). The C and N contents in the soil and plant samples were determined using a Vario EL Analyzer (Elementar, Hanau, Germany).

2.3 MCMC

We used MCMC analysis to simulate the spatial variability in water availability. The core of such analyses is to determine the Markov-chain transition probabilities. The transition probability (t) is defined as follows:

$$t_{jk}(\mathbf{h}_\Phi) = \Pr\left\{(\mathbf{x}+\mathbf{h}_\Phi)_k | (\mathbf{x})_j\right\} \quad (1)$$

where vector $\boldsymbol{x}$ is a spatial location, $\mathbf{h}_\Phi$ represents a lag (which is also a separation vector) in direction Φ, j and k represent different levels of water availability, and $(x)_j$ means that the level of water availability at point x is j. A Markov-chain model is then applied to one-dimensional categorical data in direction Φ, which assumes an exponential matrix form:

$$\mathbf{T}(\mathbf{h}_\Phi) = \exp(\mathbf{R}_\Phi \mathbf{h}_\Phi) \quad (2)$$

where $\mathbf{R}_\Phi$ denotes a transition rate matrix, $\mathbf{R}_\Phi = \begin{pmatrix} r_{11,\Phi} & \cdots & r_{1K,\Phi} \\ \vdots & \ddots & \vdots \\ r_{K1,\Phi} & \cdots & r_{KK,\Phi} \end{pmatrix}$, with entries $r_{jk,\Phi}$ representing the rate of change from category j to category k (assuming that j is present) per unit length in direction Φ.

An eigenvalue analysis must be carried out to evaluate $\exp(\mathbf{R}_\Phi \mathbf{h}_\Phi)$, which cannot be computed directly. Since the spatial variability of water availability is continuous, we used a continuous-lag Markov-chain model to describe this transition matrix:

$$\mathbf{T}(\mathbf{h}_\Phi) = \exp(\mathbf{R}_\Phi \mathbf{h}_\Phi) = \sum_{i=1}^{k} \theta_i(\Delta \mathbf{h}_\Phi)^{\mathbf{h}_\Phi/\Delta \mathbf{h}_\Phi} \mathbf{Z}_i \quad (3)$$

where $\mathbf{T}(\mathbf{h}_\Phi)$ denotes the discrete-lag transition probabilities, which can be obtained by totaling the transition count matrix $\mathbf{N}(\Delta \mathbf{h}_\Phi)$ for water availability, then dividing each row by the row sum, $\theta_i(\Delta \mathbf{h}_\Phi)$ for $i = 1$ to k denoting the eigenvalues of $\mathbf{N}(\Delta \mathbf{h}_\Phi)$, and $\mathbf{Z}_i$ denotes a spectral component matrix associated with each eigenvalue, $\theta_i(\Delta \mathbf{h}_\Phi)$.

2.4 Indices for ecological risk assessment

We used three kinds of indices to assess the ecological risk to the Yellow River Delta Wetland at different scales caused by water scarcity. Biodiversity represented the

index at a community scale, and was defined as the existence of a wide variety of vascular plant species in the wetland during a specific time period. On this basis, we calculated the biodiversity index as:

$$V_i = M_i/M \quad (4)$$

where V_i is the biodiversity of sample site i, M_i is the number of species in sample i, and M is the total number of species in the study area.

Biomass (C) represented the index at the single-plant scale, since this parameter directly reflects the ecological risk to a plant caused by insufficient water. It is calculated as follows:

$$C = C_i/S_i \quad (5)$$

where C_i is the air-dry biomass of plants in sample i and S_i is the size of the sample site.

We chose six indices at the micro-scale: uptake of nutrients, which we represented by the total nitrogen (TN), total phosphorus (TP), K, Ca, Mg, and Na contents of the plants:

$$A_i = A_{ij}/A_{i0} \ (j = 1, 2, 3) \quad (6)$$

where A_i is the absorption (uptake) index for element i, A_{ij} is the content of element i in plant species j, and A_{i0} is the content of element i in the soil. These six indices represent the utilization efficiency of the six elements, which are important for the growth and development of all three plant species.

2.5 EVR model

EVR is defined as the maximum expected loss of an ecological index at a given confidence level c, and ΔP is the possible loss of value for the ecological index:

$$\Pr\{\Delta P > \text{EVR}\} = 1 - c \quad (7)$$

In such analyses, the confidence level is usually set at 95%, so we measured the maximum loss for this level and defined the high, medium, and low risks for each index (Table 1).

2.6 Data sources and processing

We estimated the distributions of the three plant species using version 4.2 of the ENVI software (ITT Visual Information Solutions, http://www.ittvis.com/) using data extracted from Landsat TM satellite images based on supervised classification. The soil water content was simulated using version 6.0 of the GMS software (Aquaveo, http://www.aquaveo.com/) for MCMC. All data were summarized using Microsoft Excel 2007 and tested for significance using version 18 of SPSS (SPSS Inc., Chicago, IL).

For each sampling date, we classified the 130 soil water content values into three water availability levels using K-mean cluster analysis in SPSS. Based on this classification, we determined how water scarcity affected the plants using regression analysis for the eight indices. We used the coefficient of variation (CV) to represent the variation in soil water content for each species. Then we used the water availability at eight of the sampling sites (2–5 and 7–10) as inputs for the GMS software, and calculated the matrix of transition probabilities (MTP). We used the other five sites to verify the simulation results. The result of the MCMC simulation was a database with more than 2 million data points that included the soil water content for three levels of water availability, and eight indices for each of the three water availability levels for the three plant species in the spring, summer, and autumn. In the last step of this analysis, we rasterized the map of the study area using the GIS module of GMS. The resulting map contained 42 × 462 pixels, each 200 × 200 m in size. We then assigned the water availability level and values of the eight indices to each pixel in the grid.

Table 1 The ecological value at risk (EVR) of eight indices in three categories in the spring, summer, and autumn

Season	Level	Biodiversity	Biomass (kg/m^2)	Uptake of nutrients (mg/mg)					
				TN	TP	K	Ca	Mg	Na
Spring	Low	<0.1	<0.04	<40	<0.6	<0.1	<0.1	<0.4	<0.5
	Medium	0.1–0.3	0.04–0.08	40–75	0.6–1.2	0.1–0.3	0.1–0.2	0.4–0.7	0.5–2.5
	High	>0.3	>0.08	>75	>1.2	>0.3	>0.2	>0.7	>2.5
Summer	Low	<0.1	<0.7	<50	<0.4	<0.2	<0.1	<0.5	<0.5
	Medium	0.1–0.4	0.7–1.0	50–130	0.4–0.7	0.2–0.4	0.1–0.2	0.5–1.1	0.5–1.5
	High	>0.4	>1	>130	>0.7	>0.4	>0.2	>1.1	>1.5
Autumn	Low	<0.2	<0.8	<50	<0.3	<0.1	<0.03	<0.1	<1.0
	Medium	0.2–0.4	0.8–1.0	50–150	0.3–1	0.1–0.3	0.03–0.05	0.1–0.2	1–2
	High	>0.4	>1.0	>150	>1	>0.3	>0.05	>0.2	>2

3 Verification of the model

We used data from eight sample sites to simulate the distribution of soil water content in the Yellow River Delta Wetland, and used data from the remaining five sites to verify the results.

Figure 2 indicates the MTP data fit using the discrete-lag approach at a 0.1-m lag. We found that the Markov-chain data fit the measured data well in all cases and for most lag values based on the smoothness of the curves and the convergence results, which indicated that our classification of the soil water content levels was acceptable. We used MCMC to simulate the distribution of soil water content 10 times, and more than 75% of the simulated data corresponded to our field data.

4 Results and discussion

4.1 Soil water content at different depths

For the whole growing period, we obtained soil water content data from different depths at sample site 13. We compared the soil water contents at depths of 30, 50, and 100 cm from April to October in 2008 (Fig. 3). The three curves followed similar patterns, with maxima and minima

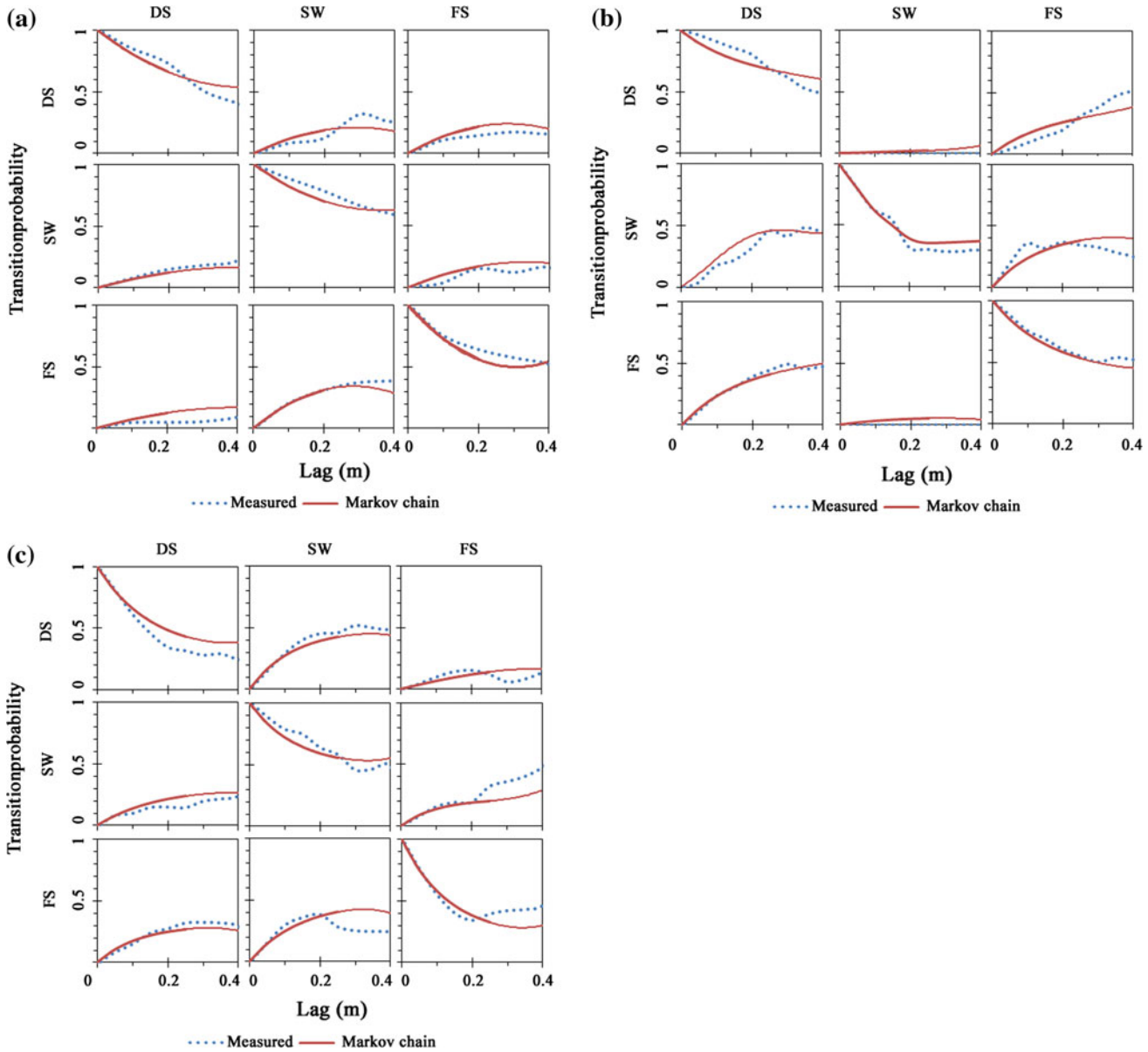

Fig. 2 Transition probabilities for different water availability levels (*DS* drought stress, *SW* sufficient water, *FS* flooding stress) as a function of the lag in **a** the spring, **b** the summer, and **c** the autumn

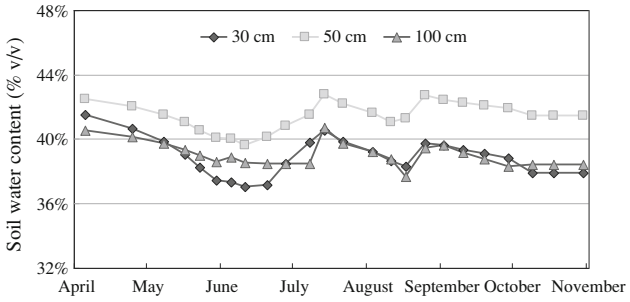

Fig. 3 Soil water content at depths of 30, 50, and 100 cm from April to October in 2008

occurring at close to the same time for all three depths. Maximum water availability occurred in late April, late July, and late August, whereas minimum water availability occurred in mid-June and mid-August. The soil water contents at depths of 30 and 50 cm were strongly correlated ($r^2 = 0.75$, $P < 0.05$). The soil water contents at depths of 30 and 100 cm were also strongly correlated ($r^2 = 0.76$, $P < 0.05$). Because of the strengths of these correlations and the fact that most plant roots were located in the top 30 cm of the soil, we chose to use the 30-cm water content for the remainder of our analysis.

4.2 Distribution of water availability in the Yellow River Delta Wetland

To reliably simulate soil water content, we classified the soil water content into three water availability levels for each season using the K-mean cluster module in SPSS, with the values adjusted to account for the relative importance of water for plant growth during each season (Table 2). The range of soil water content was smallest in the spring, and greatest in the autumn. The summer was the wettest season.

We imported the water availability level from eight of the sample sites into the GMS software, and calculated the MTP. We then calculated the water distribution by means of MCMC simulation and imported part of these data into the GMS software to represent the water availability level for each pixel in the raster map (Fig. 4). Figure 4 indicates that more sites experienced drought during the spring and autumn than during the summer. The soil water content did not show distinct spatial zonation at large scales; that is, the three water availability levels were clearly intermingled.

Table 2 The water availability levels in three seasons

Level	Soil water content (% v/v)		
	Drought stress	Sufficient water	Flooding stress
Spring	<21	21–30	>30
Summer	<25	25–35	>35
Autumn	<20	20–32	>32

4.3 The distribution and soil water content levels for the three species

Based on our field data and the Landsat TM data, we were able to define the distribution of the three plants (Fig. 5). We found that the soil water content levels differed for areas with reeds, suaeda, and saltcedar. Reeds need more water than the other two species. The reeds were able to survive at soil water contents ranging from 13 to 54%; as a result, reeds were found at sites with a mean soil water content of 33%. The suaeda needs less water than reeds, and was found at sites with a mean soil water content of 28%, which is 5% lower than the mean for reeds. Saltcedar was the most drought-tolerant species, and was found at sites with soil water content ranging from 8 to 40%, with a mean of 27%.

The CVs of soil water content for the reed, suaeda, and saltcedar sites were 0.28, 0.21, and 0.34, respectively. Based on the classification of CV values by Cambardella et al. (1994) ($CV < 0.1$, low variability; $0.1 \leq CV < 1$, medium variability; $CV \geq 1$, high variability), all three plants inhabited sites with medium variability. The saltcedar sites had the largest CV and therefore exhibited the greatest variation in soil water content, whereas suaeda inhabited sites with lower variation.

4.4 Effect of water availability on the Yellow River Delta Wetland

The different levels of water availability affected the community structure and distribution of the plants at the three scales we assessed. At the community scale, we focused on the effects of water availability on biodiversity. Figure 6 indicates that increasing water availability led to increased biodiversity, and that biodiversity increased significantly from spring to autumn at all levels of availability. We used ANOVA to test whether there was a significant difference between water levels in the same season. We found that biodiversity was generally highest in autumn when plants were under flooding stress, but the difference was not significant when the plants had sufficient water. Hence, the biodiversity differed significantly among water availability levels within a season.

At the single-plant scale, we compared the biomass of the three plants at different water availability levels (Fig. 7). Reeds had the most biomass under flooding stress, whereas suaeda and saltcedar had the highest biomass when water was sufficient. Hence, reeds could tolerate wetter conditions than suaeda and saltcedar during all three seasons. However, reeds also showed the largest decrease

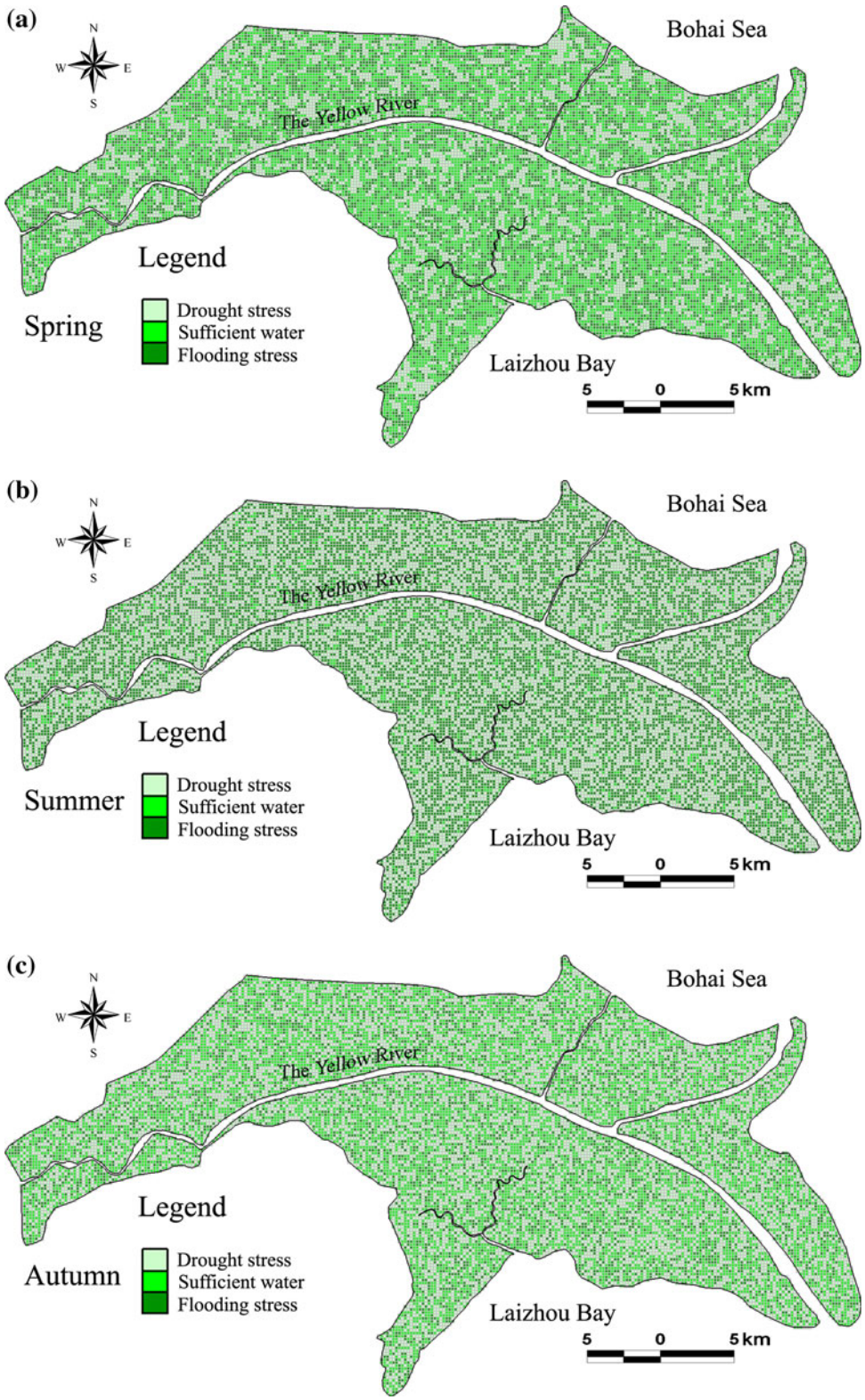

Fig. 4 Distribution of water availability levels based on the MCMC simulation in **a** the spring, **b** the summer, and **c** the autumn

in biomass under drought conditions, indicating that they were more sensitive than the other species to drought. For suaeda, biomass was significantly greater with sufficient water in all three seasons, and was significantly greater with sufficient water than under drought in summer and autumn. For saltcedar, biomass did not differ significantly between drought stress and flooding stress in the autumn, but biomass was significantly higher with sufficient water than with drought or flooding, and was significantly higher with drought than with flooding, in both summer and

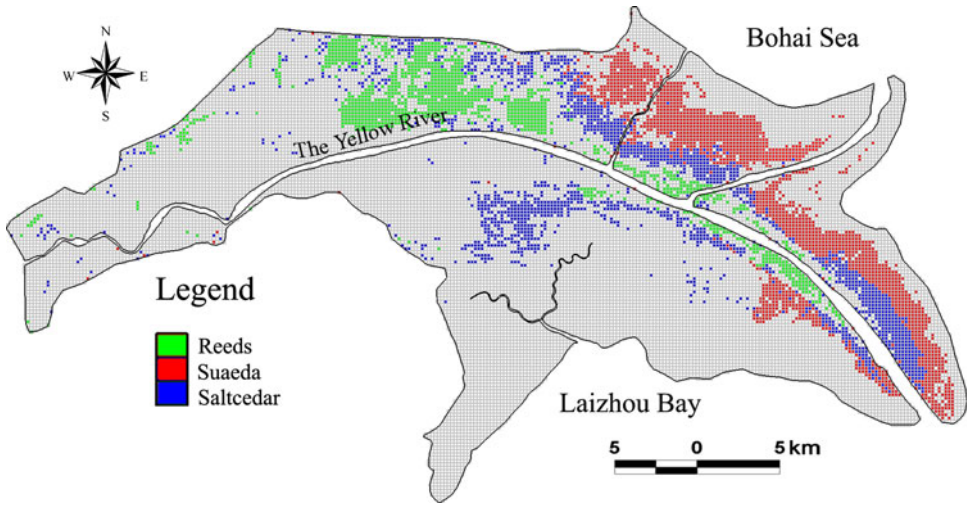

Fig. 5 The distribution of the three main plant species in the Yellow River Delta Wetland

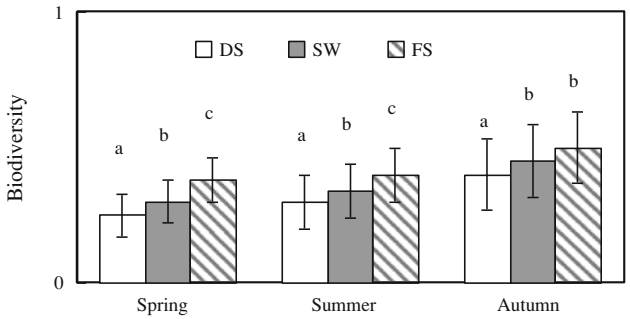

Fig. 6 Relationships between biodiversity and water availability levels (*DS* drought stress, *SW* sufficient water, *FS* flooding stress) in the spring, summer, and autumn in the Yellow River Delta Wetland. Values represent means ± SD ($n = 10$). *Bars* labeled with different *letters* differ significantly (ANOVA, $P < 0.05$) among the three water availability levels

autumn. For all three species, the net increase in biomass was greatest during the summer, and biomass subsequently declined.

At the micro-scale, we focused on the uptake of six elements by the plants. Figure 8 shows how water availability affected the uptake of these elements in each season. Reeds had the highest uptake of each element under flooding stress for most indices and most seasons, whereas saltcedar generally had the highest uptake under drought stress in all three seasons. The uptake of Mg and Na by suaeda was higher when water was sufficient, and the uptake of TP and K was higher under drought stress. The uptake of TN by suaeda was highest under drought stress in autumn, and the uptake of Ca was highest under flooding stress.

4.5 The healthy states for the three plant species

Based on the preceding discussion, we tried to identify a healthy state for each plant based on the values of the eight indices at the three scales. We found that for reeds, the indices were generally highest in the autumn, except for Na and K, which were highest under drought stress in the summer. Suaeda survived under a range of conditions. Biomass was highest with sufficient water in all seasons. The uptake of Mg and Na was highest when water was sufficient in all three seasons, whereas TP and K were highest under drought stress. Considering the biomass and uptake of TN and Ca, suaeda grew better with sufficient water. Saltcedar was unable to survive at sites where the soil water content was too high (soil water content >40%), but survived and grew well under drier conditions (i.e., soil water content <20%). Five indices for saltcedar (TN, TP, K, Ca, and Mg) were highest in all three seasons under drought stress.

Based on these results, we assumed that the optimal soil water content for healthy conditions existed under flooding stress for reeds, under sufficient water for suaeda, and under drought stress for saltcedar.

4.6 EVR at different scales

After the simulation, we assigned a level of water availability and a relative degree of health for each species to each pixel in the raster map. We calculated the EVR for each species using the 95% confidence interval. Figure 9 shows the resulting distributions of EVR for each index in the spring, summer, and autumn for this confidence interval.

At the community scale, there were 193 species of vascular plants in the study area. We observed 120 species during our investigation, but some only grew by the sides of roads, and others were rare. Only 19 species were commonly found at our sample sites: *Phragmites australis* (Cav.) Trin. ex Steud., *Suaeda salsa* (Linn.) *Pall*, *Tamarix chinensis* Lour., *Cynanchum chinense*, *Artemisia*

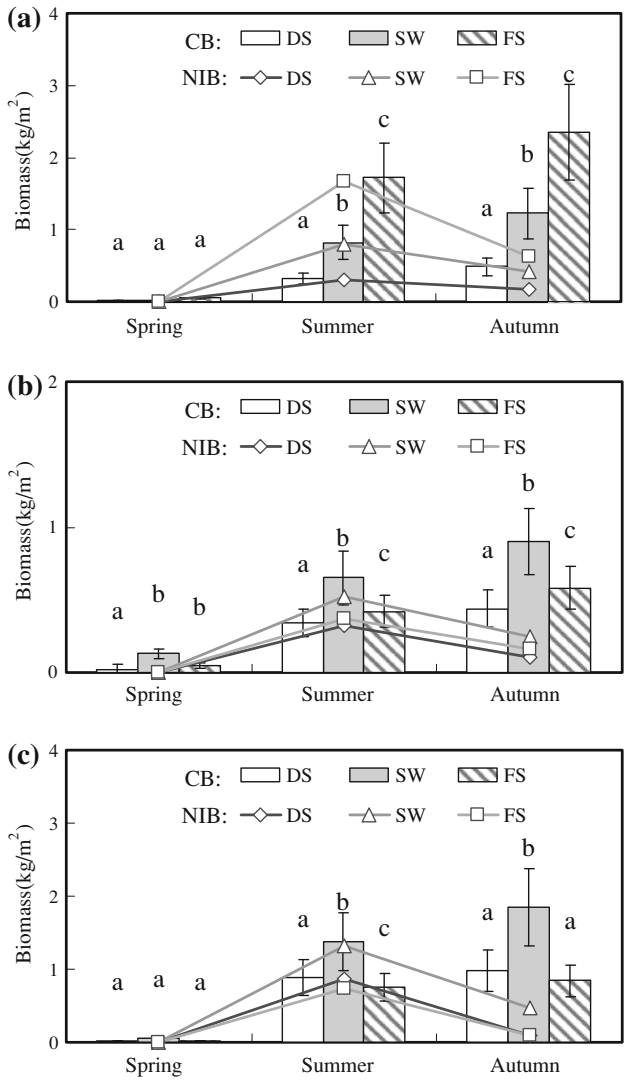

Fig. 7 Cumulative biomass (CB) and net increase in biomass (NIB) for **a** reeds, **b** suaeda, and **c** saltcedar at different water availability levels (*DS* drought stress, *SW* sufficient water, *FS* flooding stress). Values represent means ± SD ($n = 10$). *Bars* labeled with different *letters* differ significantly among the water availability levels (ANOVA, $P < 0.05$)

carvifolia, *Limonium sinense*, *Suaeda glauca*, *Cyperus glomeratus*, *Glycine soja*, *Melilotus officinalis*, *Sonchus arvensis*, *Apocynum venetum*, *Tripolium vulgare*, *Calamagrostis pseudophragmites*, *Eclipta prostrata*, *Triarrhena sacchariflora*, *Typha orientalis*, *Salix matsudana*, and *Myriophyllum spicatum*. Thus, we only used these 19 species to calculate the biodiversity of the sample sites. Figure 9a shows that the biodiversity risk increases over time, becoming much higher in autumn than in spring. The highest-risk areas are near the Bohai Sea, covering an area of about 140 km^2 in autumn. Some areas along the northeastern side of the Yellow River have a medium level of risk in spring but change to high-risk areas in autumn. Some areas along the northern bank of the Yellow River are low-risk areas in spring but change to medium-risk areas in autumn.

At a single-plant scale, biomass showed a high degree of variation (Fig. 9b). In the spring, the high-risk area for biomass was near the Bohai Sea, and covered an area of more than 72 km^2. The medium-risk area occurred along the northern bank of the Yellow River and towards the center of the study area. In the upper Yellow River delta, there is a large area with a low to medium biomass risk. In the summer, the high-risk area moves closer to the north-eastern bank of the Yellow River, and the area decreased to 63 km^2. The medium-risk area lies along the northern bank of the Yellow River, and most of the spring high-risk area near the Bohai Sea became a low-risk area by the summer. The distribution of risk levels did not change greatly in the autumn. However, the high-risk area in autumn increased to 86 km^2.

At the micro-scale, the ecological risk was represented by six uptake indices (TN, TP, K, Ca, Mg, and Na). The high-risk area for TN was less concentrated than those of the other five risks, but was mainly found between the Yellow River and the Bohai Sea in spring and summer (Fig. 9c). The high-risk area in the north-central part of the study area covered an area of 30 km^2. The risk for TP uptake differed among the seasons (Fig. 9d). The high-risk area was again located northeast of the Yellow River in the spring, and was relatively strongly concentrated. In the summer, the distribution became more dispersed. The high-risk area decreased from 71 km^2 in summer to 32 km^2 in autumn. The K uptake risk changed relatively little over time (Fig. 9e). The high-risk area was along the northern bank of the Yellow River, by the Bohai Sea, or in the north-central part of the study area and the upper reaches of the Yellow River. The high-risk area was largest (42 km^2) in the summer. The Ca uptake risk was highest in summer, when the high-risk area covered 66 km^2 (Fig. 9f). In spring, the high-risk area was located along the north-eastern side of the Yellow River, with an area of 71 km^2, as was the case for Mg (Fig. 9g). For the Na uptake risk, spring and autumn had the highest risk (Fig. 9h). In the spring, the high-risk area lay along the northern bank of the Yellow River, whereas in autumn, the high-risk area had moved towards the Bohai Sea. The risk distributions for TP, Ca, Mg, and Na were similar. The high-risk areas were found on both sides of the Yellow River or in the south-central part of the study area. The low-risk areas were located along the northern bank and upper reaches of the Yellow River, or on the northeastern side of the high-risk area by the Bohai Sea, or south towards the downstream reaches of the Yellow River.

Figure 9a shows that the biodiversity risk moves away from the shores of the river and the northern reaches towards the Bohai Sea and the southern reaches at a

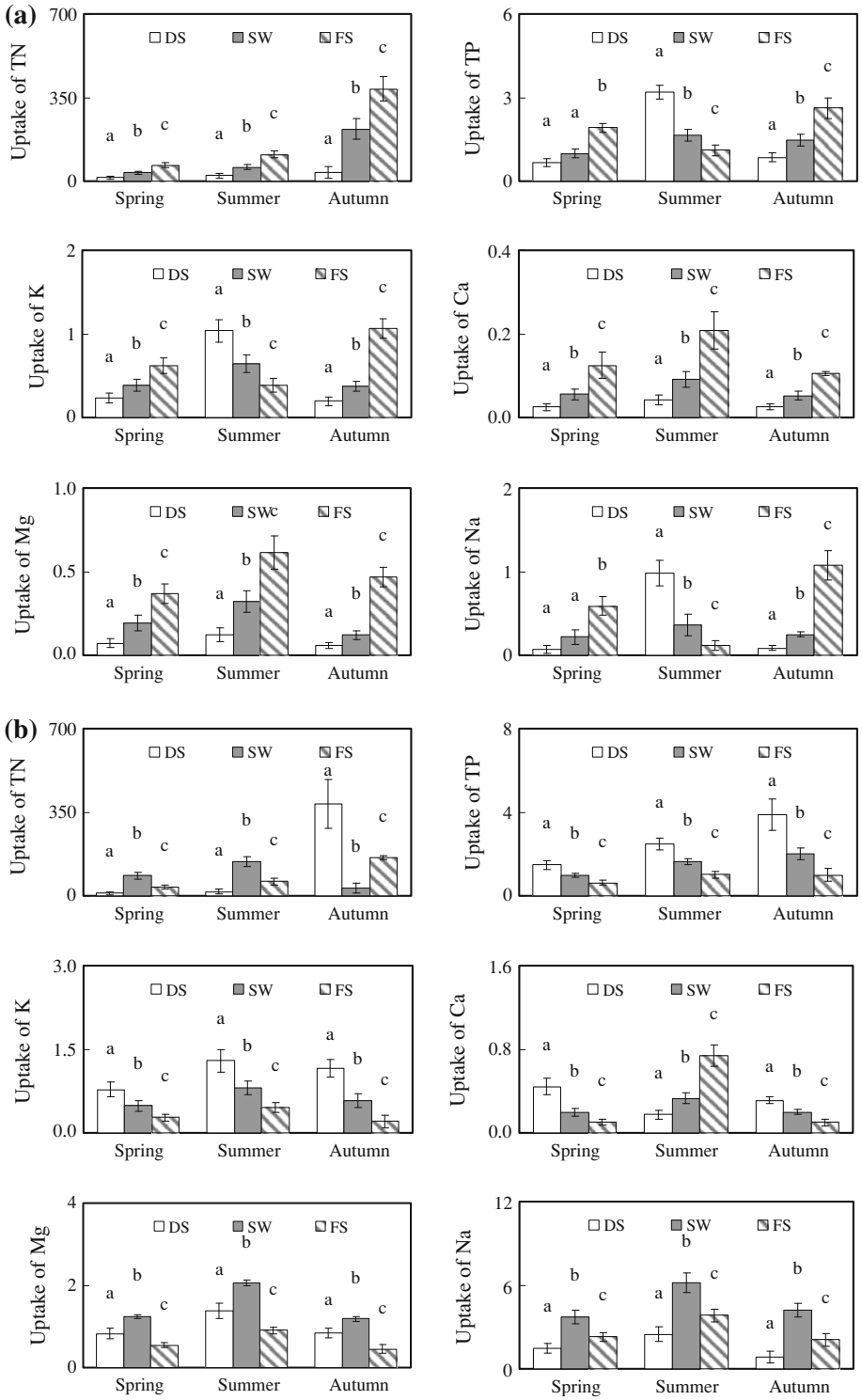

Fig. 8 Nutrient uptake indices for the total nitrogen (TN), total phosphorus (TP), K, Ca, Mg, and Na by **a** reeds, **b** suaeda, and **c** saltcedar at different water availability levels (*DS* drought stress, *SW* sufficient water, *FS* flooding stress) in the spring, summer, and autumn. Values represent means ± SD ($n = 10$). *Bars* labeled with different *letters* differ significantly (ANOVA, $P < 0.05$) among the water availability levels

community scale. That suggests the local hydrology causes water to drain towards the river (and away from the Bohai Sea) from spring to autumn as the river dries out.

In the spring, the high-risk area appears mostly where suaeda grew, whereas in summer and autumn, the high-risk area appears mostly where saltcedar grew at a single-plant scale. Spring was the droughtiest season. As new growth of suaeda needed sufficient water, the spring drought stress could place this species at risk in some areas. Because of rainfall and water–sediment regulation by the watershed's

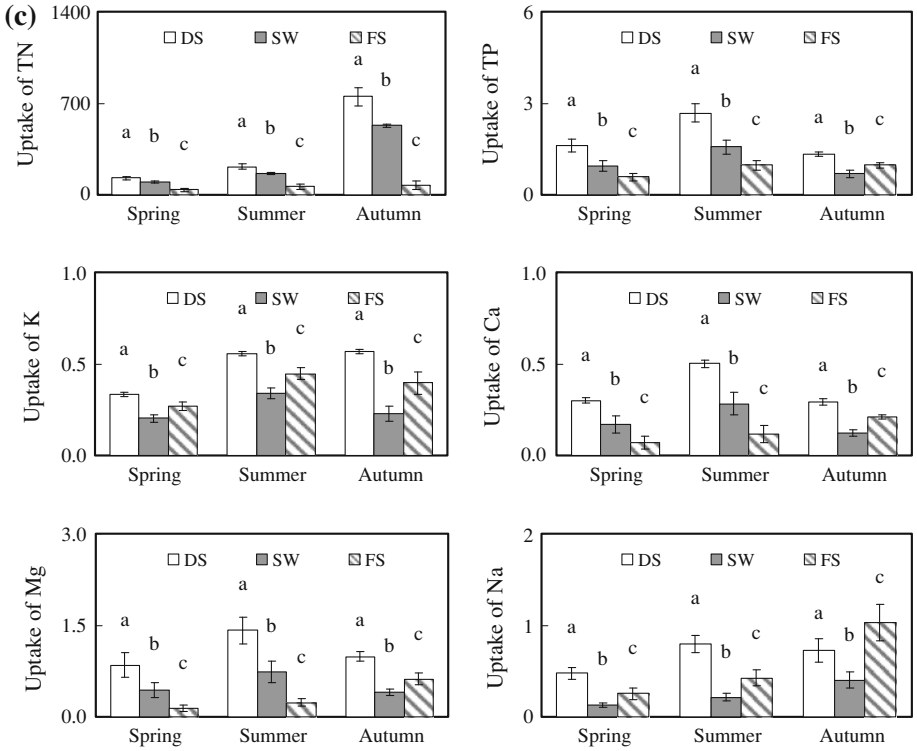

Fig. 8 continued

managers in the summer and autumn, saltcedar experienced flooding stress during these seasons, which was not the most suitable condition for its growth.

At the micro-scale, the patterns were less obvious, and the risk areas were not as concentrated as they were at the community and single-plant scales. In spring, the high-risk area was smallest for K (22 km^2), whereas the high-risk area was largest for Mg (71 km^2). In summer, the high-risk area ranged from 26 to 71 km^2, with a mean of 57 km^2. In autumn, the total high-risk area was the smallest of all three seasons, with a mean of 37 km^2.

The distributions of the ecological risk confirm that different kinds of plants need different water conditions to remain healthy, and provide a scientific foundation for the allocation of ecological flows during each season. Wetlands, including those of the Yellow River Delta, are one of the most important ecosystems in the world because of the many ecosystem services they provide. In future research, we hope to calculate the ecosystem services provided by the Yellow River Delta Wetland and changes in their values in response to different levels of water availability using the technique of ecological risk assessment. The risk to the value of these ecosystem services could provide an intuitive and straightforward result from the ecological risk assessment that will help the watershed's planners to allocate ecological flows and restore degraded areas of the wetland.

5 Conclusions

In this paper, we demonstrated how the EVR model could be used to study the ecological risks within the Yellow River Delta Wetland under different levels of water availability. Our analysis revealed the relationships between water availability levels and eight indices at three scales for three representative plant species at different times of year. We used these indices to calculate the EVR and generate a three-level distribution of ecological risk by means of MCMC simulation. The ecological risk tended to be highest in autumn at the community and single-plant scales. At a micro-scale, the summer had the highest uptake risk for TP, K, Ca, Mg, and Na, whereas the riskiest season for TN was spring. Spatially, the high-risk areas were near the Bohai Sea at a community scale and near the Bohai Sea and along the northern bank of the Yellow River at a single-plant scale. At the micro-scale, the high-risk areas were more dispersed than they were at other scales.

The analysis described in this paper provided a new method to study a wetland's ecological risk as a result of water scarcity at different scales. We introduced the EVR method, combined with MCMC simulation, and provided a way to identify areas at high risk so that watershed planners can manage the ecological flows to reduce the risks posed by fluctuations in water availability as a result of water management in regions upstream of the wetland.

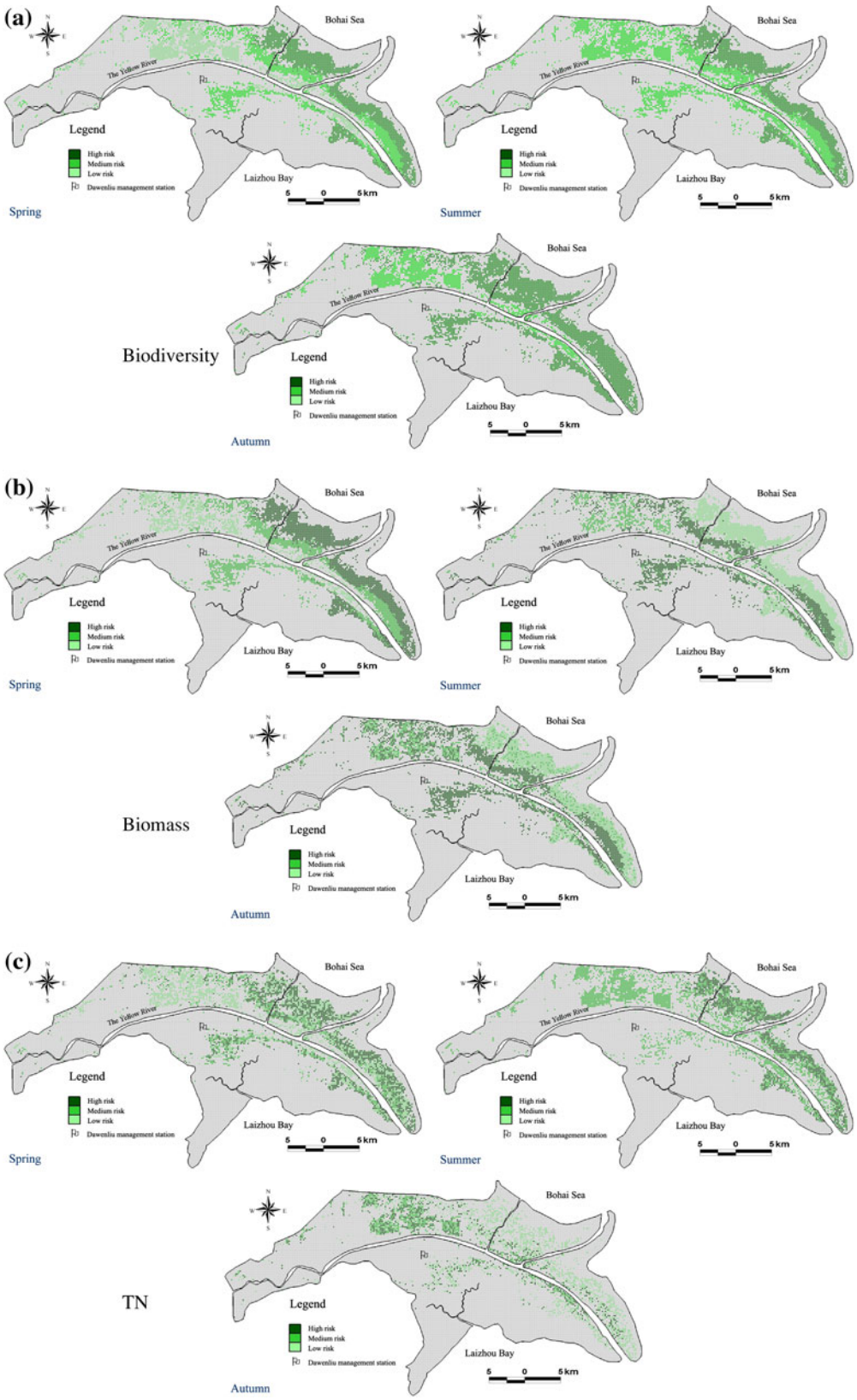

Fig. 9 Ecological risks of water scarcity for **a** biodiversity, **b** biomass, and uptake of **c** TN, **d** TP, **e** K, **f** Ca, **g** Mg, and **h** Na for a 95% confidence interval in the spring, summer, and autumn

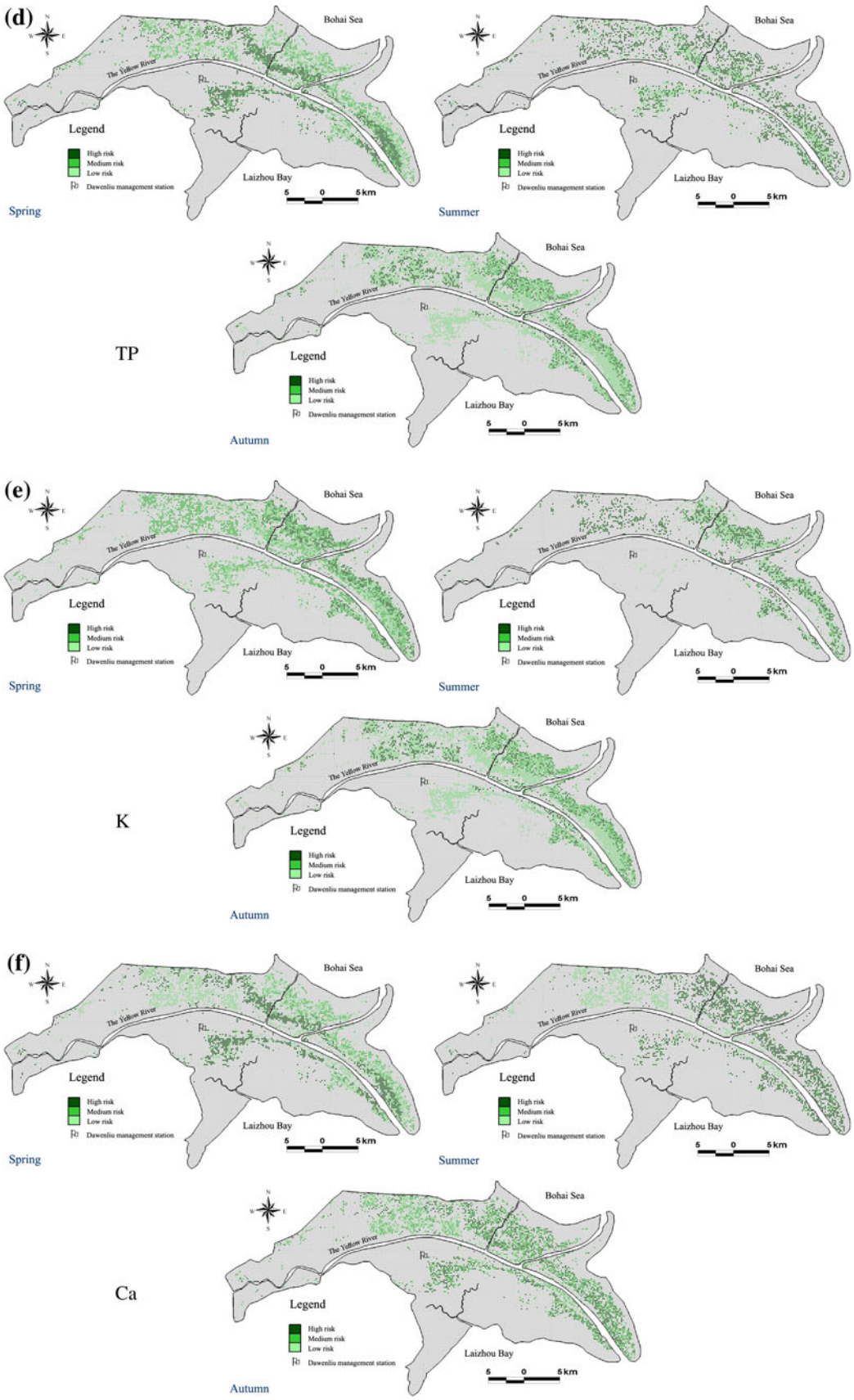

Fig. 9 continued

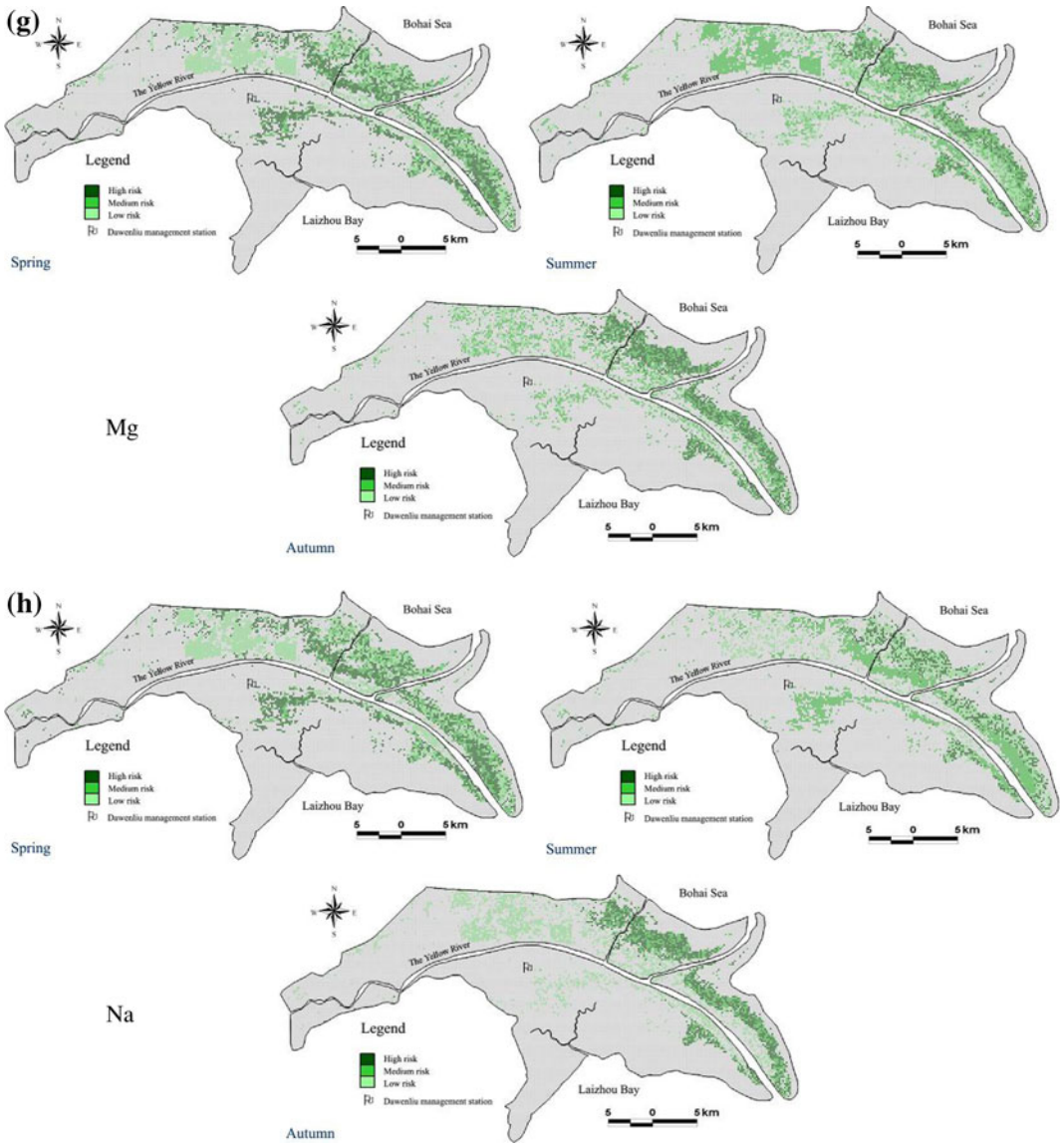

Fig. 9 continued

Acknowledgments This work was supported by the State Key Program of National Natural Science of China (Grant No. 50939001), and the National Basic Research Program of China (973) (Grant No. 2010CB951104).

References

Alexander GJ (2002) Economic implication of using a mean-VaR model for portfolio selection: a comparison with mean-variance analysis. J Econ Dyn Control 26:1159–1193

Bai JH, Wang QQ, Zhang KJ, Cui BS, Liu XH, Huang LB, Xiao R, Gao HF (2010) Trace element contaminations of roadside soils from two cultivated wetlands after abandonment in a typical plateau lakeshore, China. Stoch Environ Res Risk Assess 25:91–97

Bouma JJ, Francois D, Troch P (2005) Risk assessment and water management. Environ Model Softw 20:141–151

Brix KV, Keithly J, Santore RC, DeForest DK, Tobiason S (2010) Ecological risk assessment of zinc from stormwater runoff to an aquatic ecosystem. Sci Total Environ 408:1824–1832

Cai YP, Huang GH, Tan Q, Chen B (2009) Identification of optimal strategies for improving eco-resilience to floods in ecologically vulnerable regions of a wetland. Ecol Model 222:360–369

Cambardella CA, Moorman TB, Novak JM (1994) Field-scale variability of soil properties in Central Iowa soils. Soil Sci Soc Am J 58:1501–1511

Chen CY, Hathaway KM, Thompson DG, Folt CL (2008) Multiple stressor effects of herbicide, pH, and food on wetland zooplankton and a larval amphibian. Ecotoxicol Environ Safe 71:209–218

Dimitriou E, Karaouzas I, Sarantakos K, Zacharias I, Bogdanos K, Diapoulis A (2008) Groundwater risk assessment at a heavily industrialised catchment and the associated impacts on a peri-urban wetland. J Environ Manag 88:526–538

Dowd K (1998) Beyond value at risk: the new science of risk management. Wiley & Sons, New York

Gao F, Luo XJ, Yang ZF, Wang XM, Mai BX (2009) Brominated flame retardants, polychlorinated biphenyls and organochlorine pesticides in bird eggs from the Yellow River Delta, North China. Environ Sci Technol 43:6956–6962

He Q, Cui BS, Zhao XS, Fu HL, Liao XL (2009) Relationships between salt marsh vegetation distribution/diversity and soil chemical factors in the Yellow River Estuary, China. Acta Ecol Sinica 29:676–687 (in Chinese)

Huber NP, Bachmann D, Petry U, Bless J, Arranz-Becker O, Altepost A, Kufeld M, Pahlow M, Lennartz G, Romich M, Fries J, Schumann AH, Hill PB, Schüttrumpf H, Kongeter J (2009) A concept for a risk-based decision support system for the identification of protection measures against extreme flood events. Hydrol Wasserbewirts 53:154–159

Ji GD, Sun TH, Ni JR (2007) Impact of heavy oil-polluted soils on reed wetlands. Ecol Eng 29:272–279

Liu CM, Zhang SF (2002) Drying up of the Yellow River: its impacts and countermeasures. Mitig Adapt Strategies Glob Chang 7:203–214

Morgan Guaranry Trust Company (1996). Riskmetrics technical document, 4th edn. New York

Nabulo G, Oryem Origa H, Nasinyama GW, Cole D (2008) Assessment of Zn, Cu, Pb and Ni contamination in wetland soils and plants in the Lake Victoria basin. Int J Environ Sci Technol 5:65–74

Ni JR, Xue A (2003) Application of artificial neural network to the rapid feedback of potential ecological risk in flood diversion zone. Eng Appl Artif Intell 16:105–119

Nicolosi V, Cancelliere A, Rossi G (2009) Reducing risk of shortages due to drought in water supply systems using genetic algorithms. Irrig Drain 58:171–188

Overesch M, Rinklebe J, Broll G, Neue HU (2007) Metals and arsenic in soils and corresponding vegetation at Central Elbe river floodplains (Germany). Environ Pollut 145:800–812

Pascoe GA (1993) Wetland risk assessment. Environ Toxicol Chem 12:2293–2307

Pollard J, Cizdziel J, Stave K, Reid M (2007) Selenium concentrations in water and plant tissues of a newly formed arid wetland in Las Vegas, Nevada. Environ Monit Assess 135:447–457

Powell RL, Kimerle RA, Coyle GT, Best GR (1997) Ecological risk assessment of a wetland exposed to boron. Environ Toxicol Chem 16:2409–2414

Rumbold DG, Lange TR, Axelrad DM, Atkeson TD (2008) Ecological risk of methylmercury in Everglades National Park, Florida, USA. Ecotoxicology 17:632–641

Shi HH, Li ZZ, Li WD (2004) Model of EVR of risk management in regional ecosystem and its application. Acta Bot Boreali-Occidentalia Sinica 24:542–545 (in Chinese)

Smith SM, Gawlik DE, Rutchey K, Crozier GE, Gray S (2003) Assessing drought-related ecological risk in the Florida Everglades. J Environ Manag 68:355–366

Speelmans M, Vanthuyne DRJ, Lock K, Hendrickx F, Du LG, Tack FMG, Janssen CR (2007) Influence of flooding, salinity and inundation time on the bioavailability of metals in wetlands. Sci Total Environ 380:144–153

Srinivasan A, Shah A (2000) Improved techniques for using Monte Carlo in VAR estimation. National Stock Exchange Research Initiative, Working Paper 16

Sun T, Yang ZF, Cui BS (2008) Critical environmental flows to support integrated ecological objectives for the Yellow River Estuary, China. Water Resour Manag 22:973–989

Sun T, Yang ZF, Shen ZY, Zhao R (2009) Environmental flows for the Yangtze Estuary based on salinity objectives. Commun Nonlinear Sci Numer Simul 14:959–971

Suntornvongsaul K, Burke DJ, Hamerlynck EP, Hahn D (2007) Fate and effects of heavy metals in salt marsh sediments. Environ Pollut 149:79–91

Webby RB, Adamson PT, Boland J, Howlett PG, Metcalfe AV, Piantadosi J (2007) The Mekong—applications of value at risk (VAR) and conditional value at risk (CVAR) simulation to the benefits, costs and consequences of water resources development in a large river basin. Ecol Model 201:89–96

Xiao DN, Hu YM, Li XZ (2001) Landscape ecological research on delta wetlands around Bohai Sea. Science Press, Beijing (in Chinese)

Xie T, Liu XH, Sun T (2011) The effects of groundwater table and flood irrigation strategies on soil water and salt dynamics and reed water use in the Yellow River Delta, China. Ecol Model 222:241–252

Yang W, Yang ZF (2010) An interactive fuzzy satisfying approach for sustainable water management in the Yellow River Delta, China. Water Resour Manag 24:1273–1284

Yang ZF, Sun T, Cui BS, Chen B, Chen GQ (2009a) Environmental flow requirements for integrated water resources allocation in the Yellow River Basin, China. Commun Nonlinear Sci Numer Simul 14:2469–2481

Yang ZF, Wang LL, Niu JF, Wang JY, Shen ZY (2009b) Pollution assessment and source identifications of polycyclic aromatic hydrocarbons in sediments of the Yellow River Delta, a newly born wetland in China. Environ Monit Assess 158:561–571

Zong XY, Liu GH, Qiao YH, Cao MC, Huang C (2008) Dynamic changes of wetland landscape pattern in the Yellow River delta based on GIS and RS. In: Li G, Jia Z, Fu Z (eds) Proceedings of information technology and environmental system sciences. Publishing House of Electronics Industry, Beijing, pp 1114–1118